

Probing the morphology of epitaxial Fe/MgO discontinuous multilayers by magnetometric technique

A. Vovk^{1*}, A. García-García^{1,2}, Y.G. Pogorelov¹, J.A. Pardo^{3,4}, P. Štrichovanec⁵, C. Magén^{5,6},
P.A. Algarabel^{5,6}, J.P. Araujo¹, and G.N. Kakazei¹

¹*Departamento de Física e Astronomia, IFIMUP and IN-Institute of Nanoscience and Nanotechnology, Universidade do Porto, 4169-007 Porto, Portugal.*

²*Graphene and Nanotechnologies, Ed. CEMINEM, 50018-Zaragoza, Spain*

³*Departamento de Ciencia y Tecnología de Materiales y Fluidos, Universidad de Zaragoza, 50018-Zaragoza, Spain*

⁴*Instituto de Nanociencia de Aragón, Universidad de Zaragoza, 50018-Zaragoza, Spain*

⁵*Instituto de Ciencia de Materiales de Aragón, Universidad de Zaragoza-CSIC, 50009-Zaragoza, Spain*

⁶*Departamento de Física de la Materia Condensada, Universidad de Zaragoza, 50009-Zaragoza, Spain*

**Corresponding author ayvovk@fc.up.pt*

Abstract.

Discontinuous metal-insulator multilayers (DMIMs) are a special type of nanostructures with a layered arrangement of metallic particles sandwiched between continuous insulating layers. DMIMs exhibit moderate tunneling magnetoresistance (TMR) ratio but enhanced low-field sensitivity, which makes them promising candidates for magnetic field sensors. Recently we have grown epitaxial Fe/MgO DMIMs on MgO (001) single crystal substrates at different deposition conditions. Here, based on the analysis of magnetic isotherms in a broad temperature range, the effect of deposition temperature (T_S) on microstructure of DMIMs is being studied and compared with the results of Transmission Electron Microscopy. It is shown that metallic layers consist of flat nanoparticles whose average size decreases, and their crystallinity improves with the increase of T_S .

Keywords.

Discontinuous metal-insulator multilayers; Superparamagnetic nanoparticles; Magnetic isotherms; Tunneling Magnetoresistance.

Introduction

Magnetic discontinuous metal insulator multilayers (DMIMs) attract a lot of attention due to their potential applications as sensors with advanced response to magnetic field [1-10] and memristors [11]. DMIMs represent a special type of nanostructures where magnetic particles are arranged in layers (not distributed randomly over the volume as in the case of granular metal-insulator mixtures) and thus are considered as model systems for the magnetic interactions in 2-dimensional case and percolation studies [10, 12, 13]. It is known that a big difference in surface free energy of metals and insulators leads to non-wetting, and, in diluted regime, metallic particles of a few nanometer (nm) size encapsulated in the insulating matrix are formed [14]. One should keep in mind that the shape of particles in nanostructures could vary depending on the materials choice and deposition conditions. For example, ellipsoidal particles are formed in $\text{Co}_x\text{Cu}_{1-x}$ granular films prepared by co-evaporation, due to oblique vapor fluxes caused by wide spatial separation of the evaporation sources [15]. For $\text{CoFe}/\text{Al}_2\text{O}_3$ system (both granular [16] and DMIMs with low nominal thickness (t) of metallic layer [3, 5, 17]), Volmer-Weber island growth mechanism leads to formation of nearly spherical metallic nanoparticles embedded in amorphous insulating host. This microstructure is preserved for $\text{CoFe}/\text{Al}_2\text{O}_3$ DMIMs in a broad range of t . The metal layer becomes continuous at relatively high $t \sim 1.8$ nm. In contrary, for Fe/MgO system it was shown [18, 19] that Frank-van der Merve layer-by-layer type of growth occurs at room temperature (RT). As a result, the conditions for full coverage, i.e. formation of a continuous Fe layer, are fulfilled for its much smaller $t \sim 0.9$ nm [13, 18]. If the layer-by-layer epitaxial growth is realized for Fe/MgO system, one should expect in the discontinuous regime formation of flat rather than spherical nanoparticles. However, determination of particles size and shape in the case of nanostructured films is not a trivial task. Well established experimental techniques for structural characterization suffer serious drawbacks in this case. Both convenient X-ray diffraction (XRD) and X-ray reflectivity techniques are not too informative for particles of a few nm size in a discontinuous layer [20]. Cross-section TEM does not provide information about the shape and

size of particles in the individual layer, due to superposition of particles over the sample thickness [8]. The ion milling that is used for preparation of TEM samples for plane view studies can cause noticeable structural and compositional changes. Meanwhile, deposition of three-layer insulator/metal/insulator reference films on carbon-covered TEM grids does not reproduce the conditions of epitaxial growth on single-crystalline substrates. Thus, complementary magnetic studies become of great importance for evaluation of particle sizes and shapes in DMIMs. In this paper, an analysis of magnetic isotherms of Fe/MgO epitaxial DMIMs grown on MgO(001) substrates is reported. A comparison of the modelling results for spherical and disc-shaped particles is presented and discussed in the framework of the experimental results.

Experimental techniques

The samples were prepared by pulsed laser deposition (PLD) in an ultrahigh vacuum chamber at pressure below 10^{-8} Torr using a KrF laser producing 6 J/cm^2 fluence on the target. The deposition procedure for epitaxial MgO (3 nm)/ [Fe (0.6 nm) / MgO (3 nm)]₁₀ DMIMs on single crystal MgO (001) substrates was described in detail in Refs. 8 and 21. The substrates during the deposition were kept at $T_s = 293, 393, 453$ and 523 K . Cross-section TEM images were obtained using a FEI Tecnai F30 transmission electron microscope. Microstructure and crystal quality of the multilayers were probed by XRD using a Bruker D8 high-resolution diffractometer with $\text{Cu } K_{\alpha 1}$ radiation. Magnetic measurements were performed using a Quantum Design MPMS superconducting quantum interference device (SQUID) magnetometer equipped with Reciprocating Sample Option (RSO). Magnetization vs. applied field (M vs. H) up to 50 kOe was measured at temperatures (T) $5, 100, 200$ and 300 K . Field Cooled/Zero Field Cooled (FC/ZFC) susceptibility measurements [21] were performed at $H = 50 \text{ Oe}$ in the temperature range from 5 K to 300 K . Tunneling Magnetoresistance (TMR) was measured in the current-in-plane geometry at RT using the four-probe technique. The experimental setup was described elsewhere [13].

Results

XRD and TEM experiments confirm epitaxial growth of both MgO and Fe layers and that the multilayers present crystal coherence along the whole thickness [8]. The layered structure of the films is evident for all T_S (see Fig. 1). Fe layers of about 1 nm thickness (darker contrast) are separated by approximately 3 nm-thick MgO layers (brighter contrast). The width of XRD rocking curves decreases with increasing T_S , indicating the crystal quality improvement [8].

The saturation magnetization (M_S) of iron layer was estimated from $M(H)$ curve at $T=5K$ to be ~ 1700 emu/cm³, in good agreement with the value for bulk Fe. FC/ZFC dependencies (Fig. 2) reveal typical characteristics for an ensemble of superparamagnetic particles: (1) ZFC curves show maximum at certain temperature and (2) FC and ZFC coincide at higher temperatures and χ vs. $1/T$ dependence (not shown) is linear in agreement with the Curie law for paramagnetic relaxation. It is known [22], that small single-domain magnetic particles (if the relevant anisotropy is uniaxial) under zero applied field have freedom between two equivalent states of opposite magnetization. If the thermal energy $k_B T$ (with the Boltzmann constant k_B) is higher than the product KV , where V is the particle volume and K is the effective anisotropy constant, the magnetization vector can flip. For high enough T the thermal energy is sufficient to equilibrate the magnetization of an assembly in a time short compared with that of the experiment. Thus, the system shows paramagnetic-like behavior. In the $k_B T \ll KV$ limit the presence of the anisotropy barrier suppresses the magnetization flips and the system approaches the equilibrium within a characteristic relaxation time. The switching between these two regimes occurs at the so-called blocking temperature (T_B). In experiment, T_B is often determined as the temperature of the ZFC curve maximum. If one assumes K to be a constant for a given set of magnetic nanoparticles, the value of T_B will decrease with V . It is seen in Fig. 2 that T_B monotonically decreases from 120K to 45K with increasing T_S indicating the decrease of the particle volumes. It is to be noted, however, that in presence of shape and particle sizes distribution, the value of K could vary due to changes in surface and shape anisotropy contributions. Thus, a straightforward correlation between

T_B and V could be established only for a monodisperse ensemble of magnetic nanoparticles. The superparamagnetic behavior of our DMIMs above T_B was also confirmed by the magnetic hysteresis loops scaling. The reduced magnetization $m = M/M_S$ curves plotted against H/T for $T > T_B$ are reduced to a universal curve.

The combination of X-ray and magnetic susceptibility data allows us to conclude that the increase of T_S causes both an enhanced degree of (001) texturing of MgO and a decrease in the average Fe particle size. In this course, the TMR shows a notable enhancement [8, 21] from ~3% to ~10%. This effect was attributed to the onset of spin filtering mechanism that is more pronounced for tunnel barriers of better quality and higher degree of epitaxy. The conclusion was made [8] that the increase of T_S could be used as an alternative route to design DMIMs with improved magnetotransport properties. However, a detailed analysis of particle sizes and shape variation with T_S was not carried out yet. Below, a simple model that allows evaluating particle size and shape based on the analysis of anhysteretic magnetization reversal curves is proposed.

Modeling and Discussion

Fitting of magnetic isotherms is the most common indirect method to estimate the size of superparamagnetic particles above T_B . The equations that describe M vs. H behavior and restrictions caused by the shape anisotropy are known for a long time [23 – 26]. In the one-dimensional (1D) case, the magnetization for $T > T_B$ follows as

$$M(H,T) = M_S \tanh(x), \quad (1)$$

where $x = \mu H / (k_B T)$ with μ being the magnetic moment of a particle.

For a planar isotropic (2D) material with the magnetic field applied in the easy plane it follows as

$$M(H,T) = M_S I_1(x)/I_0(x), \quad (2)$$

where I_0 and I_1 are the zeroth and first order modified Bessel functions. Finally, for the isotropic three-dimensional (3D) case (all the directions of magnetization being equivalent), the anhysteretic function becomes

$$M(H,T) = M_S L(x), \quad (3)$$

where $L(x) = \coth(x) - 1/x$ is the Langevin function. The qualitative difference between these three dependencies is most clearly seen from their initial asymptotics: $\tanh(x) \approx x$, $I_1(x)/I_0(x) \approx x/2$, $L(x) \approx x/3$, reflecting the dimensionality of relevant magnetic moments.

The equations (1) - (3) were derived for monodisperse systems of particles. However, real ensembles of nanoparticles have certain size distributions. In the 3D case, the magnetization curves are often fitted assuming a log-normal distribution of particle sizes (PSD). This approach was proved and effectively used to determine the average particle size and PSD of magnetic granular nanostructured materials and ensembles of spherical nanoparticles [27 – 30]. Following the abovementioned routine, the initial fitting of M vs. H curves for our films was performed using an approach of spherical particles and log-normal PSD. Although a good fit to the experimental data was obtained with average diameter of spherical particles in the range of ~ 3 -4 nm, it is clearly in contradiction with the TEM images – no structural features of spherical shape with such diameters can be found across the film thickness. On the contrary, Fe particles are confined to the layers of about 1 nm thickness.

Therefore, we assumed that Fe layers in the sample consist of disc-shaped particles with in-plane diameter D and thickness t . A model structure of a single layer is presented in Figure 3. It is supposed that all the discs have the same t but variable D . We consider all the granules to contribute independently to the total magnetization. In this approximation only their individual

demagnetizing coefficients and filling factors matter, while the in-layer correlations stay irrelevant. The distance between the iron layers is 3 nm and thus the exchange interactions between them can be neglected. Thus, we do not consider any correlation between vertically packed particles in the adjusted Fe layers or an assumption that MgO spacer erases the information of the previous layer microstructure. Moreover, direct cross-section TEM studies do not provide a clear evidence that any structural correlation in vertical direction exists. This is due to the limitation of the technique, i.e. the electron beam probes several particles throughout layer thickness producing overlapping image.

For the given case, the expression for the reduced magnetization m at $T > T_B$ can be written as

$$m = \int_0^\infty \frac{\exp\left[-\frac{1}{2}\ln\left[(D/D_c)^2\right]^2/2w^2\right]}{w\sqrt{2\pi}} \left(\frac{I_1(\pi D^2 t M_S H / 4k_B T)}{I_0(\pi D^2 t M_S H / 4k_B T)}\right) \frac{dD}{D} \quad (4)$$

Here, the first factor under the integral represents the log-normal distribution for the disc's diameters with w width and D_c median diameter. The second one describes the magnetization of a disc-shaped particle with diameter D and thickness t .

The asymptotic laws for the reduced magnetization curve $m\left(\frac{H}{T}\right)$, Eq. (4), can be calculated analytically. Thus, in the low-field limit, $x = \pi D^2 t M_S H / 4k_B T \ll 1$, we approximate the ratio $I_1(x)/I_0(x) \approx x/2$ and then present low (compared to saturated) magnetization as:

$$m\left(\frac{H}{T}\right) \approx \frac{\sqrt{\pi} t M_S H}{8\sqrt{2} w k_B T} \int_0^\infty e^{-\frac{\ln^2(D/D_c)}{2w^2}} D dD =$$

$$\frac{\sqrt{\pi} t M_S H}{8\sqrt{2} w k_B T} \int_{-\infty}^\infty e^{-y^2/2w^2 - 2y} dy = \frac{\pi t D_c^2 M_S H}{8k_B T} e^{2w^2} \quad (5)$$

This can be seen as a linear function:

$$m_{lf}\left(\frac{H}{T}\right) = \kappa_{lf}\frac{H}{T} \quad (6)$$

of the argument H/T with the low-field coefficient $\kappa_{lf} = \pi t D_C^2 M_S e^{2w^2} / 8k_B$.

Otherwise, in the high-field limit, $x \gg 1$, where the above ratio is approximated as $I_1(x)/I_0(x) \approx 1 - 1/2x$, we obtain the small difference of the reduced magnetization to the full saturation ($m = 1$) as:

$$1 - m \approx \frac{\sqrt{2}k_B T}{\pi^2 w t M_S H} \int_0^\infty \frac{e^{-\frac{\ln^2(D/D_C)}{2w^2}}}{D} dD = \frac{\sqrt{2}k_B T}{\pi^{3/2} w t M_S H} \int_{-\infty}^\infty e^{-y^2/2w^2 - 2y} dy = \frac{2k_B T}{\pi t D_C^2 M_S H} e^{2w^2} \quad (7)$$

and this function is linear in the argument T/H , inverse to that eq. (6):

$$m_{hf}\left(\frac{T}{H}\right) = \kappa_{hf}\frac{T}{H}, \quad (8)$$

with high-field coefficient $\kappa_{hf} = 2k_B e^{2w^2} / \pi t D_C^2 M_S$. Then the product $\kappa_{lf}\kappa_{hf} = e^{4w^2}/4$, independent of specific parameters t , D_C and M_S , can be readily extracted from the measurements, allowing a direct estimation of the distribution width

$$w = \frac{1}{2} \sqrt{\ln(\kappa_{lf}\kappa_{hf})}. \quad (9)$$

Further on, the median diameter of the disc D_C and the average diameter $D_{avr} = D_C e^{w^2/2}$ are expressed through these coefficients as

$$D_C = \sqrt{\frac{4k_B}{\pi t M_S} \sqrt{\frac{\kappa_{lf}}{\kappa_{hf}}}} \quad (10)$$

$$D_{avr} = D_C (4\kappa_{lf}\kappa_{hf})^{1/8}. \quad (11)$$

To evaluate the PSD of disc-shaped particles using equations (9) – (11), the knowledge of both t and M_S is necessary. The value of $t \sim 1\text{nm}$ was extracted from the cross-section TEM and $M_S = 1700 \text{ emu/cm}^3$ from the low temperature ($T=5\text{K}$) magnetization measurements. The m vs. H/T fitting results at $T > T_B$ are presented in Fig.4 for the samples by the lowest ($T_S=293\text{K}$,

Fig 4(a)) and the highest ($T_S=523\text{K}$, Fig. 4(b)) deposition temperatures. The PSD w , D_C and D_{avr} parameters are summarized in Table 1 and the distribution of particle diameters in Fig. 4(c). It is seen that w and D_C monotonically decrease with increasing T_S , i.e., a more uniform distribution of smaller nanoparticles is formed. The average diameter gets reduced from ~ 5 nm to ~ 4 nm. The reduction of D_C and D_{avr} correlates with the magnetic susceptibility measurements that show decrease of T_B with increasing T_S . It is also in agreement with our previous statement [8] that increasing T_S leads to a higher nucleation density of Fe islands. A similar tendency, i.e. formation of granular-like superparamagnetic Fe/MgO structures was obtained at elevated T_S even for much thicker Fe layers (up to 1.5 nm) [18, 31].

It is worth noting a certain discrepancy between theoretically calculated and experimental curves at intermediate H/T values. This could be explained by the following. Even in the best-case the calculated ratio D_{avr}/t does not exceed ~ 5 . Though the shape of Fe particles in the DMIMs under consideration is closer to discs than to spheres, they do not represent ideal 2D particles. The model also does not account for possible distribution in t and/or deviations from the disc shape and from log-normal distribution. Nevertheless, the achieved agreement between measurements and theoretical fit with only two fitting parameters (w and D_C) is more than satisfactory.

Conclusions

Morphology of Fe nanoparticles in Fe/MgO epitaxial DMIMs has been established combining TEM investigations and magnetic measurements. A simple model that allows determination of magnetic nanoparticle sizes was developed and tested for disc-shaped particles. The comparison of the fitting results for magnetic isotherms and the direct experimental confirmation that Fe nanoparticles are confined in layers of $\sim 1\text{nm}$ thickness strongly suggests that disc-shaped particles are formed in epitaxially grown DMIMs. The modeling procedure proposed here could serve as a basis for future investigations on particle size distribution for DMIMs.

Moreover, this research demonstrates that modifying the growth conditions it is possible to control the geometrical parameters of the disc-shaped nanoparticles. Namely, the diameter of the particles can be controlled through the deposition temperature while the layer nominal thickness does through the deposition time. These open ways for engineering the heterogeneous nanostructures with desired magnetic and magnetotransport properties.

Acknowledgements

Portuguese team acknowledge support from Portuguese Foundation of Science and Technology (FCT) through the project NECL (Ref. NORTE-01-0145-FEDER-022096), “Investigador FCT” program (G.N.K.) and grant FRH/BPD/81710/2011 (A.G.-G.). This work was partially supported by Spanish Ministerio de Economía y Competitividad through project MAT2017-82970-C2, and from regional Gobierno de Aragón through project E26 including FEDER funding. The authors acknowledge access to instruments and expertise of Laboratorio de Microscopías Avanzadas (Instituto de Nanociencia de Aragón, Universidad de Zaragoza) for TEM experiments.

References

- [1] B. Dieny, S. Sankar, M.R. McCartney, D.J. Smith, P. Bayle-Guillemaud, and A.E. Berkowitz, *J. Magn. Magn. Mater.* **185**, 283 (1998).
- [2] S. Sankar, B. Dieny, and A.E. Berkowitz, *J. Appl. Phys.* **81**, 5512 (1997).
- [3] G. N. Kakazei, Yu. G. Pogorelov, A. M. L. Lopes, J. B. Sousa, S. Cardoso, P. P. Freitas, M. M. Pereira de Azevedo, and E. Snoeck, *J. Appl. Phys.* **90**, 4044 (2001).
- [4] R. Bručas, M. Hanson, P. Apell, P. Nordblad, R. Gunnarsson, and B. Hjörvarsson, *Phys. Rev. B* **81**, 224437 (2010)
- [5] G. N. Kakazei, Yu. G. Pogorelov, M. D. Costa, V. O. Golub, J. B. Sousa, P. P. Freitas, S. Cardoso, and P. E. Wigen, *J. Appl. Phys.* **97**, 10A723 (2005).
- [6] A. García-García, A. Vovk, J. A. Pardo, P. Štrichovanec, C. Magén, E. Snoeck, P. A. Algarabel, J. M. De Teresa, L. Morellón, and M. R. Ibarra, *J. Appl. Phys.* **105**, 063909 (2009)
- [7] A. García-García, A. Vovk, J. A. Pardo, P. Štrichovanec, P. A. Algarabel, C. Magén, J. M. De Teresa, L. Morellón, and M. R. Ibarra, *J. Appl. Phys.* **107**, 033704 (2010).
- [8] A. García-García, J. A. Pardo, P. Štrichovanec, C. Magén, A. Vovk, J. M. De Teresa, G. N. Kakazei, Y. G. Pogorelov, L. Morellon, P. A. Algarabel, and M. R. Ibarra, *Appl. Phys. Lett.* **98**, 122502 (2011).
- [9] O. Petravic, X. Chen, S. Bedanta, W. Kleemann, S. Sahoo, S. Cardoso, P.P. Freitas, *J. Magn. Magn. Mater.* **300**, 192 (2006).
- [10] S. Bedanta, T. Eimüller, W. Kleemann, J. Rhensius, F. Stromberg, E. Amaladass, S. Cardoso, and P. P. Freitas, *Phys Rev. Lett.* **98**, 176601 (2007).
- [11] H. Silva, H.L. Gomes, Yu.G. Pogorelov, P. Stallinga, D.M. de Leeuw, J.P. Araujo, J.B. Sousa, S.C.J. Meskers, G. Kakazei, S. Cardoso, and P.P. Freitas, *Appl. Phys. Lett.* **94**, 202107 (2009).
- [12] W. Kleemann, O. Petravic, Ch. Binek, G. N. Kakazei, Yu. G. Pogorelov, J. B. Sousa, S. Cardoso, and P. P. Freitas, *Phys. Rev. B* **63**, 134423 (2001).

- [13] A. García-García, A. Vovk, P. Štrichovanec, J. A. Pardo, C. Magén, P. A. Algarabel, J. M. De Teresa, L. Morellón, and M. R. Ibarra, *J. Phys.: Condens. Matter* **22**, 056003 (2010).
- [14] B. Abeles, P. Sheng, M. D. Coutts, Y. Arie, *Adv. Phys.* **24**, 401 (1975).
- [15] G.N. Kakazei, A.F. Kravetz, N.A. Lesnik, M.M. Pereira de Azevedo, Yu.G. Pogorelov, G.V. Bondarkova, V.I. Silantiev, J.B. Sousa, *J. Magn. Magn. Mater* **196-197**, 29 (1999).
- [16] A. Ya. Vovk, J. Q. Wang, J. He, W. Zhou, A. M. Pogoriliy, O. V. Shypil' A. F. Kravets, H. R. Khan, *J. Appl. Phys* **91**, 10017 (2002).
- [17] G.N. Kakazei, Yu.G. Pogorelov, A.M.L. Lopes, M.A.S. de Silva, J.A.M. Santos, J.B. Sousa, S. Cardoso, P.P. Freitas, E. Snoeck, *J. Magn. Magn. Mater* **266**, 62 (2003).
- [18] C. Martinez-Boubeta, C. Clavero, J. M, Garcia-Martin, G. Armelles, A. Cebollada, L. Balcells, J. L. Menendez, F. Peiro, A. Cornet and M. F. Toney, *Phys. Rev. B* **71** 014407 (2005).
- [19] Y. Park, S. Adenwalla, G. P. Felcher and S. D. Bader, *Phys. Rev. B* **52** 12779 (1995).
- [20] D. Rafaja, H. Fuess, D. Šimek, J. Kub, J. Zwick, J. Vacínová, and V. Valvoda, *J. Phys.: Condens. Matter* **14**, 5303 (2002).
- [21] A. García-García, J. A. Pardo, P. Štrichovanec, C. Magén, A. Vovk, J. M. De Teresa, G. N. Kakazei, Yu.G. Pogorelov, V. Golub, O. Salyuk, L. Morellón, P. A. Algarabel, and M. R. Ibarra, *J. Nanosci. & Nanotechn.* **12**, 7505 (2012).
- [22] C. P. Bean, *J. Appl. Phys.* **26**, 1381 (1955).
- [23] A. Raghunathan, Y. Melikhov, J. E. Snyder, and D. C. Jiles, *Appl. Phys. Lett.* **95**, 172510 (2009).
- [24] G. Bertotti, *Hysteresis in Magnetism* (Academic, London, 1998).
- [25] D. C. Jiles, S. J. Lee, J. Kenkel, and K. L. Metlov, *Appl. Phys. Lett.* **77**, 1029 (2000).
- [26] D. C. Jiles, *Introduction to Magnetism and Magnetic Materials*, 2nd ed., (Chapman & Hall, London, 1998).
- [27] E. F. Ferrari, F. C. S. da Silva, and M. Knobel, *Phys. Rev. B* **56**, 6086 (1997).

- [28] F. C. Fonseca, G. F. Goya, R. F. Jardim, R. Muccillo, N. L. V. Carreño, E. Longo, and E. R. Leite, Phys. Rev. B **66**, 104406 (2002).
- [29] J. C. Cezar, M. Knobel, and H. C. N. Tolentino, JMMM **226-230**, 1519 (2001).
- [30] B. J. Hattink, M. García del Muro, Z. Konstantinović, X. Batlle, A. Labarta, and M. Varela, Phys. Rev. B **73**, 045418 (2006).
- [31] G. Fahsold, A. Pucci, and K.-H. Rieder, Phys. Rev. B **61**, 8475 (2000).

Figure Captions

Fig. 1. TEM cross-section image of the $[\text{Fe} (0.6 \text{ nm})/\text{MgO} (3 \text{ nm})]_{10}$ DMIM deposited at 293K (a) and 523K (b) on MgO (001). Thin layers of Fe particles (darker contrast) are sandwiched between MgO layers (brighter contrast). Insets represent close-up images of Fe particles.

Fig. 2. Zero Field Cooled (squares) and Field Cooled (circles) magnetic susceptibility (χ) curves measured at $H = 50 \text{ Oe}$ for $[\text{Fe}(0.6 \text{ nm})/\text{MgO}(3 \text{ nm})]_{10}$ DMIMs deposited on MgO (001) at $T_S = 293\text{K}$ (a) and $T_S = 523\text{K}$ (b). Temperature dependence of the blocking temperature (T_B) vs. deposition temperature (T_S) is presented in panel (c).

Fig. 3. Model structure of a single layer DMIM. Magnetic Fe particles are discs with diameter D and thickness t .

Fig. 4. Magnetic hysteresis loops scaling for $[\text{Fe} (0.6 \text{ nm})/\text{MgO} (3 \text{ nm})]_{10}$ DMIMs deposited on single-crystal MgO (001) substrates at $T_S = 293\text{K}$ (a) and $T_S = 523\text{K}$ (b). The reduced magnetization m is plotted against H/T for $T > T_B$. Experimental data (points) are accompanied by the fitting curves (solid lines). The fitting parameters are summarized in Table I. Evolution of log-normal distribution of particles diameter (D) for $T_S = 293\text{K}$ and $T_S = 523\text{K}$ is shown in panel (c).

Table 1. Deposition temperature (T_S), blocking temperature (T_B), low-field coefficient (κ_{lf}) for Eq. 6 and high-field coefficient (κ_{hf}) for Eq. 8, determined from experimental data, calculated width (w) and median diameter (D_C) for log-normal distribution and average diameter (D_{avr}) of the disc-shaped particle. For the fitting procedure the values of saturation magnetization $M_S = 1700$ emu/cm³ and Fe layer thickness $t = 1$ nm were used.

T_S K	T_b K	κ_{lf} K/Oe	κ_{hf} Oe/K	w , nm	D_C , nm	D_{avr} , nm
293	120	0.19	6.0	0.62	4.3	~5.2
393	70	0.15	6.5	0.58	4.0	~4.7
453	50	0.14	6.36	0.56	3.9	~4.5
523	45	0.1	7	0.51	3.52	~4

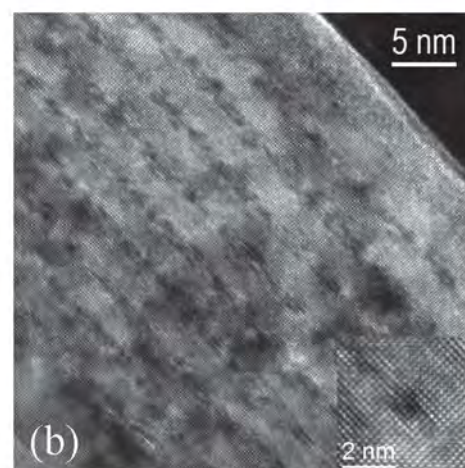
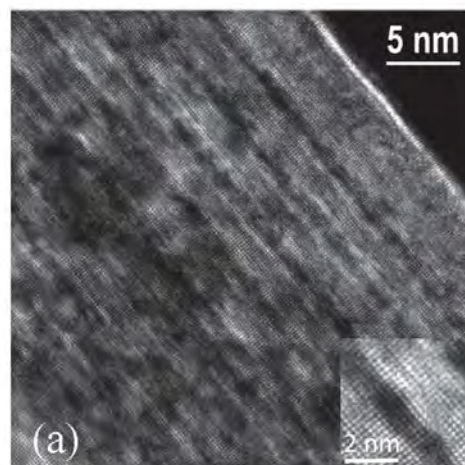


Figure 1

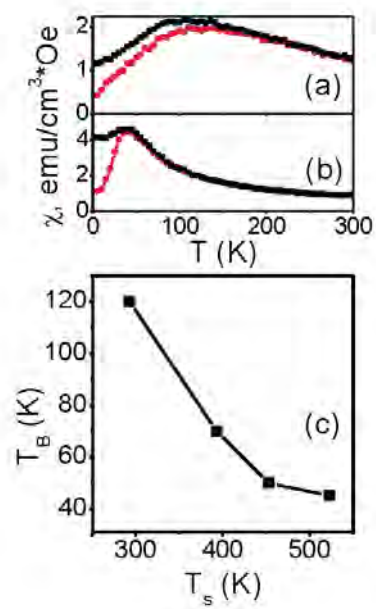


Figure 2



Figure 3

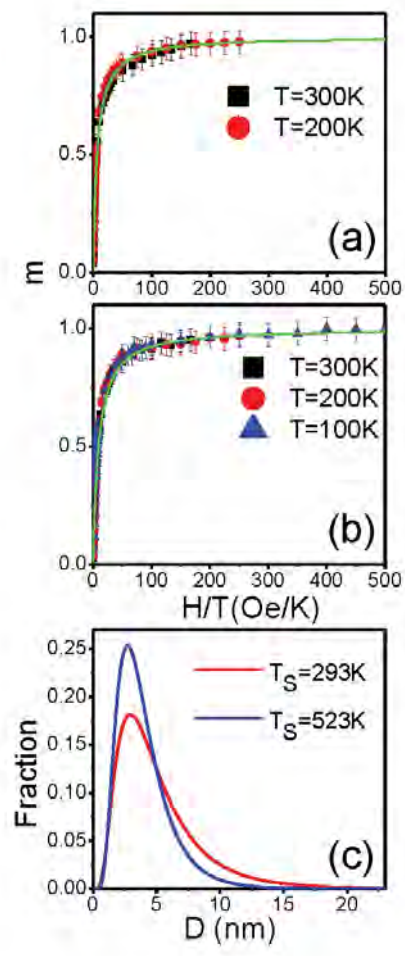


Figure 4.